JOURNAL OF SOLID STATE CHEMISTRY 73, 356–361 (1988)

Spectral Analysis of Ni^{2+} Ions in the XWO_4(X = Mg, Zn) Crystal

WANG HUISU

Physics Department, Sichuan Normal University, Chengdu, People's Republic of China

AND ZHAO SANGBO

Research Division of Chemical Physics, Sichuan Normal University, Chengdu, People's Republic of China

Received December 29, 1986; in revised form July 9, 1987

From complete ligand-field theory calculation of the absorption spectrum of nickel ions at a C_{2v} symmetry site, the absorption spectrum of Ni^{2+} ions in a XWO_4 crystal is reanalyzed. According to these results, two spin-allowed absorption bands in the infrared region of Ni^{2+} spectra can be derived and the observed polarizations of spectra can be explained when spin–orbit coupling is taken into account. From the Gaussian deconvolution of the observed band it is shown that an absorption peak around 11,000 cm^{-1} should exist. In our calculation, the number of adjustable parameters is decreased and the calculated results are better than that of R. Borromei, G. Ingletto, L. Oleari, and P. Day (*J. Chem. Soc. Faraday Trans. 2* **78**, 1705 (1982)).

1. Introduction

The luminescent properties of the divalent metal ion tungstates including some doped transition metal ions have been widely investigated (*1–3*). The absorption spectra of Ni^{2+} and Co^{2+} in $ZnWO_4$ and $MgWO_4$ have been measured by Borromei *et al.* (*4, 5*) and theoretical analysis of the absorption spectra has also been done by them. Considering that Ni^{2+} and Co^{2+} in such crystals are all located at a C_{2v} low symmetry crystal site, Borromei *et al.* calculated the positions of absorption spectra by taking into account effects of electronic interaction and C_{2v} crystal-field interaction. In the case of Co^{2+}, the theoretical result is in good agreement with experimental observation (*5*); but in Ni^{2+}, according to crystal-field parameters (Δ, η, ϑ, ε) introduced by Borromei *et al.* (*4*), all of the observed absorption bands are hard to calculate and are not quite in agreement with experimental observation (see Table I).

At the same time, three calculated bands $^3A_1$, $^3A_2$, and $^3B_1$ belong to X, Y polarization and electric dipole forbidden, respectively (see Table 1), so that the strong bands along Z-axis polarization will not appear in the 10,000 cm^{-1} region. However, from the polarization absorption spectra measured by Borromei *et al.*, we have seen that two separate strong bands both contain a component having Z polarization. Therefore, the calculation given by Borromei *et al.* obviously disagrees in this respect with the observed results. We think the reason is that Ni^{2+} is a strong paramagnetic ion, and the

0022-4596/88 $3.00

spin–orbit coupling effect should be taken into account (in Co^{2+}, this spin–orbit coupling intensity due to paramagnetism is smaller than that in Ni^{2+}). Therefore this article goes further to calculate the influence of spin–orbit coupling on spin triplet energy matrix of Ni^{2+} and to get the complete ligand field energy spectrum. Then the polarized absorption spectrum measured by Borromei *et al.* is reanalyzed and we further explain some regularities of the Ni^{2+} spectrum in such types of crystals.

2. The Energy Matrices, Including Spin–Orbit Interaction in the Direct Product Representations

The contributions of electrostatic interaction, crystal field, and spin–orbit coupling effects to the energy matrices of the $d^2(d^8)$ system are discussed here. Based on the strong field scheme and the C_{2v} energy matrices derived by Borromei *et al.* (*4*), a simple method (*6*) is used to write energy matrices of spin–orbit direct product representation of C_{2v} point group for spin triplet states of the $d^2(d^8)$ system. The results are as follows (italic symbols with a prime),

$$A_1'(9) = \begin{bmatrix} \mathbf{T}_2'(4) & & \\ & \mathbf{A}_1'(2) & \\ & & \mathbf{E}'(3) \end{bmatrix}$$

$$A_2'(7) = \begin{bmatrix} \mathbf{T}_1'(3) & \\ & \mathbf{T}_2'(4) \end{bmatrix}$$

$$B_1'(7) = \begin{bmatrix} \mathbf{T}_1'(3) & \\ & \mathbf{T}_2'(4) \end{bmatrix}$$

$$B_2'(7) = \begin{bmatrix} \mathbf{T}_1'(3) & & \\ & \mathbf{A}_2'(1) & \\ & & \mathbf{E}'(3) \end{bmatrix}, \quad (1)$$

where each boldface symbol stands for the energy matrics corresponding to the spin–orbit direct product irreducible representation of 0*. In the diagrams above and following, the numbers in parentheses stand for the orders of submatrices. Since we take the Griffith (*7*) standard bases of 0* to

TABLE I

THE RESULTS OF THE SPECTRA ANALYSIS

This article		Borromei *et al.* (*4*)		
Transition	$E_{calc.}$ (cm^{-1})	Transition $^3B_2\rightarrow$	$E_{calc.}$[a] (cm^{-1})	$E_{obs.}$[d] (cm^{-1})
	Ground state splitting			
A_2'	0			
B_1'	2.993			
A_1'	4.235			
$A_1', A_2', B_1'\rightarrow$				
B_2'	6,410	$^3A_1$	6,514(Y)	6,330(s) (Y,Z)
A_2'	6,464			
B_1'	6,546			
A_1'	6,630			
B_2'	6,702			
A_2'	6,868	$^3A_2$	6,824(X)	
A_1'	7,277			
B_2'	7,278	$\nrightarrow{}^3B_1$[c]	7,558	7,200(s)
B_1'	7,285			(Z,Y,X)
B_1'	11,044			11,000(s)[b] (Z,X,Y)
A_1'	11,158			
A_2'	11,177			
B_2'	11,322	$\nrightarrow{}^3B_1$[c]	11,242	
A_1'	11,388			
B_1'	11,452			
A_2'	12,053	$^3B_2$	11,750(Z)	12,050(s) (Z,X,Y)
B_2'	12,063			
A_1'	12,078	$^3A_2$	12,382(X)	12,200(s) (Z,X,Y)
$^1A_1$	13,680	$^1A_1$	13,562	13,605
$^1B_1$	13,916	$^1B_1$	13,614	13,790
$^1B_2$	20,015	$^1A_1$	19,754	19,800
$^1A_1$	20,025	$^1A_2$	20,009	
$^1A_2$	20,400	$^1B_2$	20,508	20,400
A_1'	21,527			
B_1'	21,683			
A_2'	21,787	$^1A_1$	21,724	21,275
$^1A_1$	22,196	$\nrightarrow{}^3B_1$[c]	21,820	22,000(s)
B_2'	22,103			(Z,X)
B_1'	22,417	$^3B_2$	22,199(Z)	
A_1'	22,524			
A_2'	22,925	$^3A_2$	22,857(X)	22,850(s) (Z,Y)
A_1'	23,015			
B_2'	23,070			
$\lambda\langle r^2\rangle = 4.5\ a_0^2$	$\Delta = 6768$	$\Delta = 7000\ cm^{-1}$		
$\lambda\langle r^4\rangle = 19.0\ a_0^4$	$\eta = 443$	$\eta = 293\ cm^{-1}$		
$B = 882.9\ cm^{-1}$	$\vartheta = -422$	$\vartheta = 721\ cm^{-1}$		
$C = 3721\ cm^{-1}$	$\varepsilon = 602$	$\varepsilon = 100\ cm^{-1}$		
$\xi = -569\ cm^{-1}$		$B = 870\ cm^{-1}$		
		$C = 3610\ cm^{-1}$		

[a] The parameters have been suitably selected. There are some mistakes in the paper of Borromei *et al.* (*4*) (see text).

[b] See Fig. 1.

[c] Electric dipole forbidden.

[d] s: strong band. X, Y, Z polarization orientation.

be the starting point, then in the case of considering only the electrostatic energy and the 0 component of the crystal field, the strong field matrices Γ' of $0^*(d^2\text{–}d^8)$ are in block-diagonal forms derived from those of $0(d^2\text{–}d^8)$ as follows:

$$\begin{aligned}
\boldsymbol{A}_1'(2) &= [{}^3T_1(2)] \\
\boldsymbol{A}_2'(1) &= [{}^3T_2(1)] \\
\boldsymbol{E}'(3) &= \begin{bmatrix} {}^3T_1(2) & \\ & {}^3T_2(1) \end{bmatrix} \\
\boldsymbol{T}_1'(3) &= \begin{bmatrix} {}^3T_1(2) & \\ & {}^3T_2(1) \end{bmatrix} \\
\boldsymbol{T}_2'(4) &= \begin{bmatrix} {}^3T_1(2) & & \\ & {}^3T_2(1) & \\ & & {}^3A_2(1) \end{bmatrix}. \qquad (2)
\end{aligned}$$

Substitute the parts of Eq. (2) into Eq. (1) and add the matrices in Eq. (1) to the corresponding matrices of the pure C_{2v} component of the crystal field potential and of the spin–orbit coupling effects which occur only in the matrices of Eq. (1). This produces the spin-triplet state complete strong field matrices of $C_{2v}^*(d^2\text{–}d^8)$ which are given under Appendix.

3. Numerical Results

Because of indeterminacy in choosing the four crystal field parameters (Δ, η, ϑ, ε) introduced by Borromei *et al.*, it is very inconvenient to perform the calculation. But these parameters are all related to one-electron crystal field matrix elements (*4*). Since the structure of XWO_4 crystal has been measured (*8, 9, 4*), these elements have been calculated using structural data for the C_{2v} crystal site and expressions derived by Zhao *et al.* (*10*). The results are calculated as (in Borromei coordinate now)

$$\begin{aligned}
a_1 &= 160.93\lambda\langle r^2\rangle - 133.92\lambda\langle r^4\rangle \\
b_2 &= 160.93\lambda\langle r^2\rangle + 207.31\lambda\langle r^4\rangle \\
b_1 &= -194.73\lambda\langle r^2\rangle - 141.93\lambda\langle r^4\rangle \\
a_2 &= 33.80\lambda\langle r^2\rangle - 151.62\lambda\langle r^4\rangle \\
2a_1 &= -160.93\lambda\langle r^2\rangle + 220.15\lambda\langle r^4\rangle,
\end{aligned}$$

where λ is the effective charge of each ligand, the units of $\lambda\langle r^2\rangle$, $\lambda\langle r^4\rangle$, and the one-electron crystal field matrix elements are a_0^2, a_0^4, and cm^{-1}, respectively. By suitably selecting $\lambda\langle r^2\rangle$ and $\lambda\langle r^4\rangle$, corresponding values of the four parameters Δ, η, ϑ, and ε may be calculated. In the XWO_4(X = Mg, Zn) crystal, $\lambda\langle r^2\rangle = 4.5a_0^2$, $\lambda\langle r^4\rangle = 19a_0^4$ are selected here, so $\Delta = 6768\ cm^{-1}$, $\eta = 443\ cm^{-1}$, $\vartheta = -422\ cm^{-1}$, $\varepsilon = 602\ cm^{-1}$. Using the normalization constant N of one-electron molecule orbit, which is introduced by Curie *et al.* (*11*), we can take $B = N^4B_0$, $\zeta = N^2\zeta_0$, approximately. For free ion Ni^{2+}, $B_0 = 1084\ cm^{-1}$ and $\zeta_0 = 649\ cm^{-1}$ (*7*). By suitably selecting $N = 0.95$ and $C = 4.215B$, then substituting all of the parameters into spin-triplet state energy matrices (see Appendix), the results of the energy splitting are obtained as in Table I. Obviously the fitted excitation energies are in good agreement with experimental observation.

4. Spectral Analysis

Low-temperature polarized absorption spectra of $ZnWO_4$($MgWO_4$) crystals doped with Ni^{2+} have been accurately measured by Borromei *et al.* (*4*). In a comparison of the calculated results in which spin–orbit coupling has been taken into account to results in (*4*), the effect of strong paramagnetism of Ni^{2+} on the spin-allowed transitions in the infrared region is very important. From this, our theoretical calculation has given some transitions which approximate observed bands at ca. 6330 and 7200 cm^{-1}. However, those very weak transitions (hard to distinguish) in the 5900–6000 cm^{-1} region cannot be attributed to Ni^{2+}. Mostly, perhaps these weak peaks can be weak absorption from other impurities (such as Fe^{2+}) in crystal.

Because spin–orbit interaction has led to

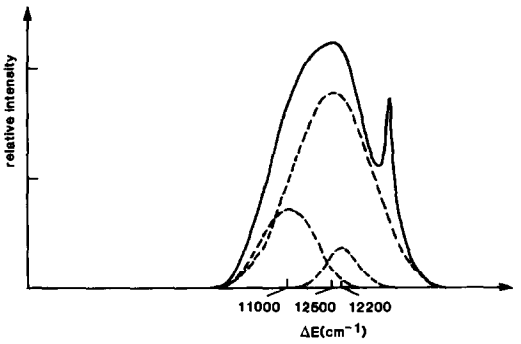

FIG. 1. Gaussian deconvolution of the observed absorption band in 10,000–12,500 cm^{-1} region. $ZnWO_4:Ni^{2+}$ (E//b), —; Gaussian peak, ---.

the mixing of various states, the constraint upon electric-dipole forbidden transitions no longer exists. Various polarizations of absorption occur. This fact is in agreement with the observed results. This theoretical analysis predicts that a rather strong absorption at 11,000 cm^{-1} should be seen in the spectrum, but it is not mentioned by Borromei *et al.* In fact, the shape of the absorption band of $ZnWO_4:Ni^{2+}$ in the range 10,000–15,000 cm^{-1} is not Gaussian on either left- or right-hand sides. According to Gaussian deconvolution (*12*), this band is the superposition of three Gaussian bands at 11,000, 12,050, and 12,200 cm^{-1}, respectively (see Fig. 1).

We have found that a series of absorptions, which arise from splittings caused by spin–orbit coupling, corresponds to the same observed absorption band. Therefore, every observed band must be a Gaussian convolution of several Gaussian absorption bands. This fact has explained that the total form of all strong absorption peaks which are observed by Borromei *et al.* do not have the standard Gaussian distribution form.

Moreover, there is also some improvement in parameter selection in our complete energy matrix of the C_{2v}^{*} point group of the $d^2(d^8)$ system, and the calculated results are also better than that of Borromei *et al.* (*4*). Similar problems appear in Ni^{2+} spectra of $NiNb_2O_6$ single crystals (*13*). The method mentioned in this article can also be used for $NiNb_2O_6$, and this work has been reported in another article (*14*).

References

1. A. E. NOSENKO AND D. L. L. FUTORSKII, *Opt. Spektrosk.* **34,** 286 (1973).
2. M. L. REYNOLDS, W. E. HAGSTON, AND G. F. J. GARLICK, *Phys. Status Solidi* **30,** 735 (1968).
3. A. E. NOSENKO, M. PASHKOVSKII, AND D. L. L. FUTORSKII, *Opt. Spektrosk.* **34,** 160 (1970).
4. R. BORROMEI, G. INGLETTO, L. OLEARI, AND P. DAY, *J. Chem. Soc. Faraday Trans. 2* **77,** 2249 (1981).
5. R. BORROMEI, G. INGLETTO, L. OLEARI, AND P. DAY, *J. Chem. Soc. Faraday Trans. 2* **78,** 1705 (1982).
6. S. B. ZHAO, H. S. WANG, AND K. W. ZHOU, *J. Phys. C* **19,** 2729 (1986).
7. J. S. GRIFFITH, "The Theory of Transition-Metal Ions," Cambridge Univ. Press, Tables A27, A33 (1961).
8. O. S. FILIPENKO, E. A. POBEDIMSKAYA, V. I. PONOMAREV, AND N. V. BELOV, *Sov. Phys. Crystallogr. Engl. Transl.* **13,** 933 (1969).
9. O. S. FILIPENKO, E. A. POBEDIMSKAYA, AND N. V. BELOV, *Sov. Phys. Crystallogr. Engl. Transl.* **13,** 127 (1969).
10. S. B. ZHAO, H. S. WANG, K. W. ZHOU, AND X. S. CHEN, *Sci. Bull. (China)* **31,** 731 (1986).
11. D. CURIE, C. BARTHOU, AND B. CANNY, *J. Chem. Phys.* **61,** 3048 (1974).
12. A. M. HOFMEISTER AND G. R. ROSSMAN, *Phys. Chem. Miner.* **11,** 213 (1984).
13. R. BORROMEI, G. INGLETTO, L. OLEARI, AND P. DAY, *J. Chem. Soc., Faraday Trans. 2* **79,** 847 (1983).
14. H. S. WANG AND S. B. ZHAO, "XXV ICCC Book of Abstracts," A186, Nanjng (1987).

THE SPIN–TRIPLET ENERGY MATRICES OF C_{2v}^* STRONG FIELD TERMS OF $d^2(d^8)$ ELECTRON SYSTEM

C_{2v}^*	O_η (d^2)	O_η^*									
	$^3T_1$ (t_2^2)	T_2'	$2\Delta + 3B - \eta - \frac{1}{2}\xi$	$-\frac{\xi}{2} \pm 6B$	$-\frac{\sqrt{3}}{2}\xi$	0	$-\sqrt{\frac{3}{2}}\vartheta$	0	$-\frac{\vartheta}{\sqrt{3}}$	0	0
	· (t_2e)	·		$\Delta + 12B + \eta + \frac{\varepsilon}{2} + \frac{\xi}{4}$	$-\frac{\sqrt{3}}{2}\varepsilon - \frac{\sqrt{3}}{4}\xi$	0	0	$-\frac{\vartheta}{\sqrt{6}}$	0	$-\frac{\vartheta}{2\sqrt{3}}$	$\frac{\sqrt{3}}{2}\vartheta$
	$^3T_2$ (t_2e)	·			$\Delta + \eta - \frac{\varepsilon}{2} - \frac{\xi}{4}$	$-\sqrt{2}\xi$	0	$\frac{\vartheta}{\sqrt{2}}$	0	$\frac{\vartheta}{2}$	$\frac{\vartheta}{2}$
	$^3A_2$ (e^2)	·				0	0	0	0	0	0
A_1'	$^3T_1$ (t_2^2)	A_1'					$2\Delta + 3B + \xi$	$\xi \pm 6B$	$-\sqrt{2}\eta$	0	0
	· (t_2e)	·						$\Delta + 12B - \frac{1}{2}\xi$	0	$\sqrt{2}\eta + \frac{\varepsilon}{\sqrt{2}}$	$-\frac{\varepsilon}{\sqrt{2}}$
	$^3T_1$ (t_2^2)	E'							$2\Delta + 3B + \eta - \frac{1}{2}\xi$	$-\frac{\xi}{2} \pm 6B$	$\frac{3}{2}\xi$
	· (t_2e)	·								$\Delta + 12B - \eta - \frac{\varepsilon}{2} - \frac{\xi}{4}$	$-\frac{\varepsilon}{2} + \frac{3}{4}\xi$
	$^3T_2$ (t_2e)	·									$\Delta + \eta - \frac{\varepsilon}{2} + \frac{1}{4}\xi$

C_{2v}^*	O_η (d^2)	O_η^*							
	$^3T_1$ (t_2^2)	T_1'	$2\Delta + 3B + \frac{1}{2}(\eta - \vartheta + \xi)$	$\frac{\varepsilon}{2} \pm 6B$	$\frac{\sqrt{3}}{2}\xi$	$\frac{1}{2}(3\eta + \vartheta)$	0	0	0
	· (t_2e)	·		$\Delta + 12B - \frac{1}{2}(2\eta + \varepsilon + \vartheta + \xi)$	$\frac{\sqrt{3}}{4}(\varepsilon - \vartheta) + \frac{\sqrt{3}}{4}\xi$	0	$-\frac{3}{2}\eta - \frac{1}{2}(3\varepsilon - \vartheta)$	$\frac{\sqrt{3}}{4}(\vartheta - \varepsilon)$	0
	$^3T_2$ (t_2e)	·			$\Delta - \frac{1}{2}\eta + \frac{1}{2}(\varepsilon + \vartheta + \xi)$	0	$\frac{\sqrt{3}}{4}(\vartheta - \varepsilon)$	$-\frac{3}{2}\eta + \frac{1}{2}(3\varepsilon - \varepsilon)$	0
A_2'	$^3T_1$ (t_2^2)	T_2'				$2\Delta + 3B + \frac{1}{2}(\eta - \vartheta - \xi)$	$-\frac{1}{2}\xi \pm 6B$	$-\frac{\sqrt{3}}{2}\xi$	0
	· (t_2e)	·					$\Delta + 12B - \frac{\eta}{2} + \frac{1}{4}(\vartheta - \varepsilon + \xi)$	$\frac{\sqrt{3}}{4}(\varepsilon - \vartheta) - \frac{\sqrt{3}}{4}\xi$	0
	$^3T_2$ (t_2e)	·						$\Delta - \frac{\eta}{2} + \frac{1}{4}(\varepsilon + \vartheta - \xi)$	$-\sqrt{2}\xi$
	$^3A_2$ (e^2)	·							

C_{2v}^*	O_η (d^2)	O_η^*							
	$^3T_1$ (t_2^2)	T_1'	$2\Delta + 3B + \frac{1}{2}(\eta + \vartheta + \xi)$	$\frac{\xi}{2} \pm 6B$	$\frac{\sqrt{3}}{2}\xi$	$\frac{1}{2}(3\eta - \vartheta)$	0	0	0
	· (t_2e)	·		$\Delta + 12B - \frac{\eta}{2} + \frac{1}{4}(\vartheta - \varepsilon - \xi)$	$\frac{\sqrt{3}}{4}(\vartheta + \varepsilon + \xi)$	0	$-\frac{3}{4}\eta - \frac{1}{4}(3\varepsilon + \vartheta)$	$-\frac{\sqrt{3}}{4}(\vartheta + \varepsilon)$	0
B_1'	$^3T_2$ (t_2e)	·			$\Delta - \frac{\eta}{2} + \frac{1}{4}(\varepsilon - \vartheta + \xi)$	0	$-\frac{\sqrt{3}}{4}(\vartheta + \varepsilon)$	$-\frac{3}{4}\eta + \frac{1}{4}(3\varepsilon + \vartheta)$	0
	$^3T_1$ (t_2^2)	T_2'				$2\Delta + 3B + \frac{1}{2}(\eta + \vartheta - \xi)$	$-\frac{\xi}{2} \pm 6B$	$-\frac{\sqrt{3}}{2}\xi$	0
	· (t_2e)	·					$\Delta + 12B - \frac{\eta}{2} - \frac{1}{4}(\varepsilon - \vartheta + \xi)$	$\frac{\sqrt{3}}{4}(\varepsilon - \vartheta) - \frac{\sqrt{3}}{4}\xi$	0
	$^3T_2$ (t_2l)	·						$\Delta - \frac{\eta}{2} + \frac{1}{4}(\varepsilon - \vartheta - \xi)$	$-\sqrt{2}\xi$
	$^3A_2$ (e^2)	·							0

C_{2v}^*	O_η (d^2)	O_η^*							
	$^3T_1$ (t_2^2)	T_1'	$2\Delta + 3B - \eta + \frac{1}{2}\xi$	$\frac{1}{2}\xi \pm 6B$	$\frac{\sqrt{3}}{2}\xi$	0	ϑ	0	0
	· (t_2e)	·		$\Delta + 12B + \eta + \frac{1}{2}\varepsilon - \frac{1}{2}\xi$	$\frac{\sqrt{3}}{4}\xi - \frac{\sqrt{3}}{2}\varepsilon$	$-\frac{\vartheta}{\sqrt{2}}$	0	$\frac{\vartheta}{2}$	$\frac{\vartheta}{2}$
B_2'	$^3T_2$ (t_2e)	·			$\Delta + \eta - \frac{\varepsilon}{2} + \frac{1}{4}\xi$	$-\frac{\vartheta}{\sqrt{6}}$	0	$-\frac{\sqrt{3}}{2}\vartheta$	$\frac{\vartheta}{2\sqrt{3}}$
	· (t_2e)	A_2'				$\Delta - \frac{\xi}{2}$	0	$-\frac{\varepsilon}{\sqrt{2}}$	$\frac{\varepsilon - 2\eta}{\sqrt{2}}$
	$^3T_1$ (t_2^2)	E'					$2\Delta + 3B - \eta - \frac{1}{2}\xi$	$-\frac{\xi}{2} \pm 6B$	$\frac{3}{2}\xi$
	· (t_2e)	·						$\Delta + 12B + \eta + \frac{\varepsilon}{2} - \frac{1}{4}\xi$	$\frac{\varepsilon}{2} + \frac{3}{4}\xi$
	$^3T_2$ (t_2e)	·							$\Delta - \eta + \frac{\varepsilon}{2} + \frac{\xi}{4}$

Note. A-$8B + 1.2\Delta$ has been subtracted from all diagonal elements. $\xi > 0$ and the lower value is adopted for d^2; $\xi < 0$ and the upper value is adopted for d^8. The definitions of all parameters are the same as in Borromei *et al.* (*4*).